ROS

RESEARCH ARTICLE

Zinc Oxide Nanoparticles Enhance Oxidative Stress in CHO Cells

N. Prajitha, S.S. Athira, and P.V. Mohanan

Toxicology Division, Biomedical Technology Wing, Sree Chitra Tirunal Institute for Medical Sciences and Technology, Poojapura, Trivandrum 695 012, Kerala, India

Correspondence: mohanpv@sctimst.ac.in (P.V.M.)

Prajitha N et al. Reactive Oxygen Species 8(24):341–357, 2019; ©2019 Cell Med Press
http://dx.doi.org/10.20455/ros.2019.867
(Received: June 24, 2019; Revised: August 1, 2019; Accepted: August 3, 2019)

ABSTRACT | Zinc oxide nanoparticles (ZnONPs) are developed by industries for various novel and innovative applications like cosmetics, textiles, electronics, and pharmaceutics. Zinc is an essential mineral required in human diet, as it is involved in a number of biochemical reactions and organ functions in the body. There is a greater concern over its extended usage and subsequent toxicity/safety issues to living beings. There are several in vitro and in vivo studies highlighting the toxic effects of ZnONPs in various aspects. The present study focuses on the interaction of ZnONPs with Chinese hamster ovary (CHO) cells, a widely used cell line for recombinant protein manufacturing and biopharmaceutical research. Our results showed that ZnONPs caused toxicity in CHO cells in a concentration- and time-dependent manner. In agreement with this finding, oxidative stress analysis by the DCFH-DA assay also confirmed a concentration- and time-dependent elevation in reactive oxygen species (ROS) generation in ZnONPs-exposed cells. Concomitant alterations in cytoskeletal arrangement and lysosomal dysfunctions were also obtained in cells treated with ZnONPs (50 and 100 µg/ml). FACS analysis after Annexin/PI staining of treated cells confirmed apoptotic and necrotic cell death. Hence, the present study demonstrated that ZnONPs are able to cause apoptotic and necrotic cell death in CHO cells likely via an oxidative stress-dependent mechanism.

KEYWORDS | Apoptosis; CHO cells; Lysosomes; Mitochondria; Molecular toxicity; Nanoparticles; Nuclear condensation; Oxidative stress; Reactive oxygen species; Zinc oxide

ABBREVIATIONS | AO/EtBr, acridine orange-ethidium bromide; DAPI, 4,6-Diamidino-2-phenylindole; DCF, dichlorofluorescein; DCFH-DA, 2,7-dichlorofluorescein diacetate; FBS, fetal bovine serum; JC-1, 5,5′,6,6′-tetrachloro-1,1′,3,3′-tetraethylbenzimi-dazolylcarbocyanine iodide; MMP, mitochondrial membrane potential; MTT, 3-(4,5-Dimethylthiazol-2-yl)-2,5-diphenyltetrazolium bromide; NPs, nanoparticles; PBS, phosphate-buffered saline; ROS, reactive oxygen species; ZnONPs, zinc oxide nanoparticles

CONTENTS

©2019 AIMSCI Inc. All Rights Reserved.

1. INTRODUCTION

Nanotechnology is an emerging field of science that involves far-reaching research on the fabrication and application of nanoscale materials. Nanomaterials have obtained significant scientific attention by their smallest size (1–100 nm), largest surface area, tunable shapes (nanotubes, nanowires) and other physicochemical properties [1]. The widespread application of nanoparticles (NPs) concomitantly increases the risk of toxicity in humans via inhalation, ingestion, implantation, or dermal route. Toxic effects of these NPs mainly depend on their concentration and route of exposure. Long-term exposure to NPs can directly damage the cells or can be accumulated within various organ systems [2].

The field of research on nanomaterials has led to the development of several biomedical applications like imaging techniques and anti-cancer therapies with high degree of sensitivity and effectiveness. Zinc oxide nanoparticles (ZnONPs) are considered as one of the suitable candidates for drug delivery, gene delivery, imaging techniques, and as a biosensor [3]. Because of their excellent semiconducting, photo catalytic, UV blocking, antibacterial, and cross-linking properties, ZnONPs are preferred in textile, rubber, electronic, pharmaceutical, and cosmetic industries [4]. Due to the reason of widespread usage and exposure to these NPs, it is important to study their toxicity and safety aspects in biological system. There are many studies proving the toxicity of ZnONPs in soil and marine ecosystems [5, 6]. Several in vitro and in vivo toxicity studies are available regarding organ specific toxicity of ZnONPs including photo toxicity [7], nephrotoxicity [8], hepatotoxicity [9], neurotoxicity [10], and inhalation toxicity [11].

It was reported that toxicity exerted by ZnONPs is mainly due to their ability to generate reactive oxygen species (ROS) and associated oxidative stress within cells [12, 13]. Being an active ingredient used in the manufacturing of daily life products, ZnONPs require adequate safety evaluation before getting applied. Among the susceptible organs of nanotoxicity, reproductive organs like the ovary need an exceptional level of consideration because of the probable

©2019 AIMSCI Inc. All Rights Reserved.

toxic outcomes it could generate in preceding generations. Even though there exist a plethora of literatures describing toxic response of ZnONPs in various tissue models, reports in the context of reproductive tissues are scarce. In view of this, the present study addresses the cellular level nanotoxic response of ZnONPs in CHO cell line.

2. MATERIALS AND METHODS

2.1. Chemicals

High glucose Dulbecco's modified Eagles medium (DMEM) (Gibco) and fetal bovine serum (FBS) were from Gibco/Thermo Fisher Scientific (Waltham, MA, USA). Phosphate-buffered saline (Ca^{2+} and Mg^{2+}free; PBS), antibiotic and antimycotic solution (10,000 µg/ml of streptomycin, 10,000 units/ml of penicillin, and 25 µg/ml of Fungizone®Antimycotic), and 3-(4,5-dimethylthiazol-2-yl)-2,5-diphenyltetrazolium bromide (MTT) were from Sigma-Aldrich (St. Louis, MO, USA). Neutral red dye was from Sisco Research Laboratories (Maharashtra, India). Rhodamine phalloidin was from Abcam (Cambridge, UK). 2,7-Dichlorofluorescein diacetate (DCFH-DA) and Alexa Flour 488 Annexin V/Dead cell apoptosis kit were from Invitrogen (Carlsbad, CA, USA). Coomassie brilliant blue stain was from Merck (Kenilworth, NJ, USA). 4,6-Diamidino-2-phenylindole (DAPI) and acridine orange were from Himedia (Mumbai, India).

2.2. Physico-Chemical Characterization

In-house synthesized ZnONPs by wet precipitation method were used for the entire study. Characterization of the particles by transmission electron microscopy (TEM), X-ray diffraction, and Fourier transform infra-red spectroscopy was previously reported by Syama et al. [14]. Briefly, zinc nitrate (14.02 g) was used as the precursor of zinc ion and sodium hydroxide (3.24 g) as the reducing agent. The solution of $Zn(NO_3)_2$ was added dropwise to the heated NaOH solution with constant stirring. The reaction was kept undisturbed for 2 h. The precipitated ZnONPs were washed 5 times with deionized water followed by absolute ethanol and freeze-dried. The size of the particle was found to be around 6–8 nm and showed characteristic crystallinity (**Figure 1-I**).

2.3. CHO Cell Culture

The CHO cell line was purchased from the National Centre for Cell Science (NCCS, Pune, India). Cells were incubated at 37ºC with 5% CO_2 in high glucose DMEM medium containing 10% FBS and 1% antibiotic-antimycotic stock solution. Freshly prepared ZnONPs of different concentrations were used for the entire study.

2.4. Cell Viability Assessment

2.4.1. MTT Assay

MTT assay depends on the colorimetric measurement of the purple colored formazan formed from the reduction of MTT by NAD(P)H-dependent cellular oxidoreductases present in metabolically active cells [15]. In brief, 1×10^4 cells were seeded into a 96-well plate and incubated for 24 h at 37ºC and 5% CO_2. ZnONPs prepared in various concentrations (5, 15, 25, 50, and 100 µg/ml) in DMEM were added to each well and incubated for 3, 6, and 24 h. 100 µl of MTT reagent was added to each well and incubated for 4 h. After solubilizing the formed formazan crystals using 100 µl dimethyl sulfoxide (DMSO), the reaction mixture was kept in dark for 30 min at room temperature. Spectrophotometric measurement was taken at 540 nm using a multi-well plate reader (ELx 808 ultra-microplate reader, BioTek Instruments, Winooski, VT, USA). Cell Viability was expressed in percentage (%) with respect to control cells.

2.4.2. Neutral Red Uptake Assay

Neutral red uptake assay is a sensitive method used for the measurement of cell viability based on the ability of living cells to uptake and incorporate the vital dye within their lysosomes [16]. Cells were seeded at a density of 1×10^4 cells/well and incubated for 24 h at 37ºC and 5% CO_2. Afterwards, ZnONPs of varying concentrations (5, 15, 25, 50, and 100 µg/ml) were added to cells and incubated for 3, 6, and 24 h. Following incubation, 100 µl of 0.4% neutral red reagent was added to each well and allowed to react for 3 h. The dye taken up by the active cells was solubilized by 100 µl desorbing agent (1% glacial acetic acid, 50% ethanol, and 49% distilled water) and kept in dark for 30 min. Absorbance was read at 540 nm using a microplate reader (ELx 808

©2019 AIMSCI Inc. All Rights Reserved.

ultra-microplate reader, BioTek Instruments). All the values were expressed in percentage of viability.

2.5. Morphology Analysis

2.5.1 Assessment of Cellular Morphology by Coomassie Brilliant Blue Staining

The cellular morphology of CHO cells was analyzed by Coomassie Brilliant blue staining. Cells were seeded at an initial density of 1×10^5 cells/well on cover slips placed in a 6-well plate. After overnight incubation, cells were treated with different concentrations (5, 25, 50, and 100 µg/ml) of ZnONPs for 24 h. Cells were washed with ice-cold PBS and fixed using 4% formaldehyde for 15 min. The cells were then stained with Coomassie Brilliant blue solution (0.5% in 4:1 of methanol to acetic acid) for 10 min. After washing with PBS, slides were observed under a compound microscope (Olympus CX31, Japan).

2.5.2 Cytoskeleton Disruption by Rhodamine-Phalloidin Staining

Rhodamine-phalloidin was used to analyze the effect of ZnONPs on cytoskeletal integrity of CHO cells by staining F-actin filaments [17]. In brief, 1×10^4 cells were seeded into a cover slip placed in a six-well plate and incubated overnight. ZnONPs of various concentrations (5, 50, and 100 µg/ml) were added to the cells for 24 h. Following PBS wash, cells were fixed using 4% formaldehyde and permeabilized using 0.1% Triton X-100 for 1 min. The actin filaments were stained using rhodamine-phalloidin for 15 min and the nuclei were counterstained with DAPI (5 µg/ml) for 1 min. Cells were washed with PBS and observed using blue (461 nm) and red (620 nm) filters under a fluorescent microscope (Axio Scope.A1, Carl Zeiss, Germany).

2.6. DCFH-DA Assay for Intracellular ROS Generation

DCFH-DA is a non-fluorescent compound which is readily permeable to the cell membrane. Intracellular esterase hydrolyzes DCFH-DA and release DCFH. ROS generated inside the cells oxidize DCFH to form a highly fluorescent compound dichlorofluorescein (DCF) [18]. After incubation of cells seeded at a density of 1×10^4 cells/well, 100 µl of DCFH-DA (2.5 µM) was added to each well and allowed to incubate for 45 min in dark. The cells were treated with different concentrations of ZnONPs (5, 15, 25, 50, and 100 µg/ml) for 3, 6, and 24 h. 0.09% hydrogen peroxide (H_2O_2) was used as positive control. Fluorescence measurement was taken at 485 nm/528 nm (excitation/emission) wavelengths, respectively, using a microplate reader (Plate Chameleon TM V, Hidex, Finland). Qualitative analysis of DCFH-DA-stained cells after 24 h exposure to ZnONPs was analyzed using a green filter (550 nm) under a fluorescent microscope (Axio Scope.A1, Carl Zeiss)

2.7. Assessment of Mitochondrial Membrane Potential (MMP) by JC-1 Dye

The cyanine dye JC-1 (5,5′,6,6′-tetrachloro-1,1′,3,3′-tetraethylbenzimi-dazolylcarbocyanine iodide) is widely used for the discrimination of energized and de-energized mitochondria. In de-energized mitochondria with low MMP, it exists as monomers emitting green fluorescence. The dye undergoes inter conversion of green fluorescence to red during accumulation in energized mitochondria in response to their higher membrane potential [19]. In a 6-well plate, coverslips seeded with 1×10^4 cells/well were treated with 5, 15, 25, 50, and 100 µg/ml of ZnONPs for 24 h. After incubation, cells were washed twice with PBS and stained with JC-1 dye for 30 min at 37°C. Cell images were taken using green (550 nm) and red (635 nm) filters under a fluorescent microscope (Axio Scope.A1, Carl Zeiss).

2.8. Lysosomal Integrity by Acridine Orange Staining

Acridine orange staining is a novel method for the assessment of lysosomal membrane integrity upon exposure to various foreign particles [20]. Cells were seeded on a cover slip at a density of 1×10^5 cells/well and were cultured for 24 h at 37°C. After incubation, medium was discarded and the cells were treated with different concentrations of ZnONPs (5, 25, 50, and 100 µg/ml) for 24 h. Cells were stained with acridine orange (6 µg/ml) for 5 min and the excess stain was removed by washing the cells with PBS. Acid vesicles within treated and untreated cells were observed using red (635 nm) and green (550 nm) filters under a fluorescence microscope (Axio Scope.A1, Carl Zeiss).

©2019 AIMSCI Inc. All Rights Reserved.

2.9. Nuclear Condensation by DAPI

DAPI is one of the best nuclear binding dyes widely employed for the determination of nuclear condensation within the cell [21]. 1 × 10^5 cells/well were seeded onto cover slips placed in a 6-well plate and incubated with ZnONPs of different concentrations: 5, 25, 50, and 100 µg/ml for 24 h. Then the cells were washed with PBS and fixed using 4% formaldehyde for 15 min. Cells were stained with 5 µg/ml of DAPI for 1 min in dark and the cell boundary was counterstained with 5 µg/ml acridine orange. Excess stain was removed by PBS washing. Nuclear condensation was observed using green (550 nm) and blue (461 nm) filters under a fluorescence microscope (Axio Scope. A1, Carl Zeiss).

2.10. Apoptosis/Necrosis Assays

2.10.1. Acridine Orange-Ethidium Bromide (AO/EtBr) Staining for Analysis of Cell Necrosis

AO/EtBr dual staining is a conventional method for the analysis of cellular apoptosis or necrosis [22]. Simply, 1 × 10^6 cells were seeded into a 6-well plate. After 24 h incubation, the cells were treated with 5, 15, 25, 50, and 100 µg/ml of ZnONPs for 24 h. The cells were trypsinized and centrifuged at 525 *g* for 5 min. The pellets were stained using 1 µg/ml of AO/EtBr stain for 5 min. The cells were observed using green (550 nm) and red (635 nm) filters under a fluorescent microscope (Axio Scope. A1, Carl Zeiss).

2.10.2. Annexin/PI Flow Cytometric Analysis of Apoptosis/Necrosis

Live/dead assay was carried out using the Annexin V/PI cell apoptosis kit to analyze whether the cells undergo apoptosis/necrosis, after treating with varying concentrations of ZnONPs for 24 h. Flipping occurs for phosphatidyl serine residing in the inner leaflet of cells towards outer leaflet of plasma membrane, so that annexin V could specifically bind it. PI stains only dead cells that indicate the loss of membrane integrity. Assay was carried out as per manufacturer's instructions. Briefly, cells were seeded (1 × 10^6 cells/well) in a 6-well plate. After exposing cells with ZnONPs for 24 h, cells were harvested by trypsinization. Cell pellets were obtained after centrifugation and washed with PBS; followed by resuspension in 500 µl annexin binding buffer (ABB). 5 µl of annexin V (1:1 dilution) and 1 µl of PI were added to the suspension and made up to 200 µl using ABB. Cells were incubated for 30 min in dark at room temperature and then analyzed by flow cytometry (Guava Easycyte, Millipore, Burlington, MA, USA).

2.11. Statistical Analysis

Experiments were done in triplicates. MTT, neutral red and DCFH-DA assay results were expressed as mean ± standard deviation. Statistical analysis was done using student's t-test. P values of < 0.05 and < 0.01 were considered as statistically significant and indicated as * and **, respectively.

3. RESULTS

3.1. Cell Viability

Cell viability was assessed by MTT assay after exposure of 5, 15, 25, 50, and 100 µg/ml of ZnONPs in CHO cells for 3, 6, and 24 h. The result showed a concentration- and time-dependent decrease in cellular viability at 50 and 100 µg/ml (**Figure 1-II**).

The lysosomal activity status of CHO cells after exposure to ZnONPs were analyzed by neutral red uptake assay. A concentration- and time-dependent reduction in cell viability similar to that detected by MTT assay was observed after exposure to ZnONPs (**Figure 1-IIIA**). **Figure 1-IIIB** (**a–d**) shows representative microphotographs of neutral red uptake by the cells after exposure to ZnONPs at 0, 25, 50, and 100 µg/ml, respectively, for 24 h.

3.2. Cellular Morphology

Coomassie brilliant blue is a protein binding stain used for the analysis of cellular morphology. Low concentrations of ZnONPs (5 to 15 µg/ml) showed characteristic epithelial cell morphology similar to control cells. Cellular morphology changed at the concentration of 25 µg/ml of ZnONPs and rounding up of cells was visible from 50 µg/ml onwards. 90% cells were detached from the culture plate at 100 µg/ml of ZnONPs (**Figure 2a**).

Cytoskeletal integrity of the CHO cells was studied using rhodamine-phalloidin staining of actin fil-

©2019 AIMSCI Inc. All Rights Reserved.

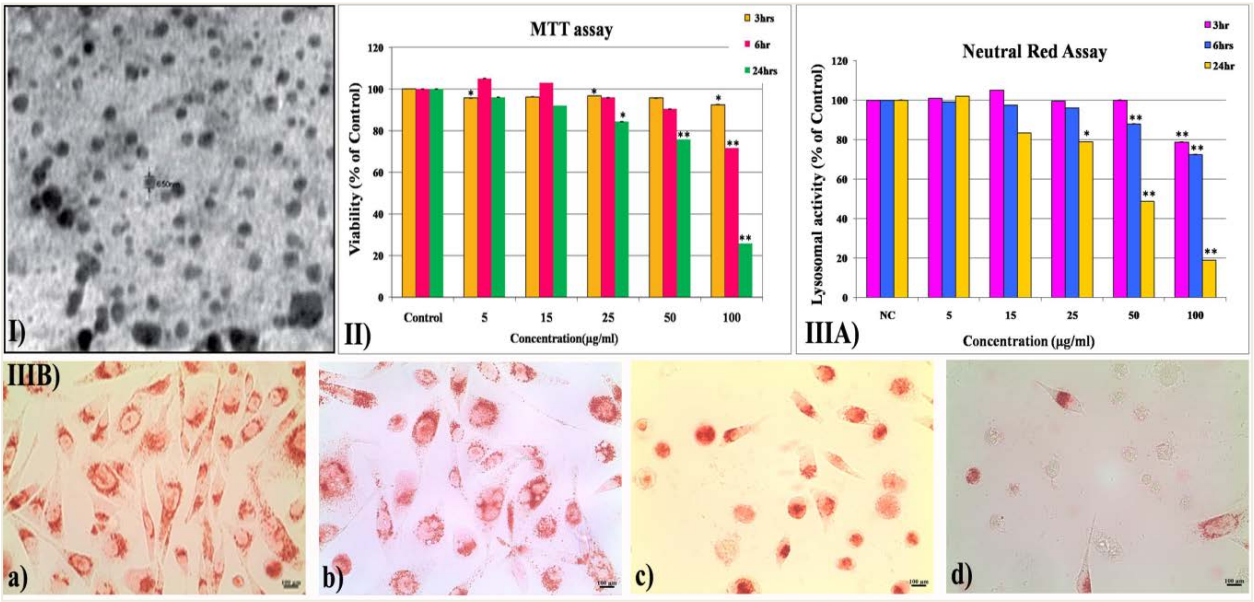

FIGURE 1. Transmission electron microscopy (TEM) image of ZnONPs and the effects of ZnONPs on CHO cell viability. I: A representative TEM image of ZnONPs. II: Assessment of cell viability after treatment with ZnONPs for 3, 6, and 24 h by the MTT assay. IIIA: Quantitative analysis of neutral red uptake by control and treated cells. IIIB: Representative microphotographs of neutral red uptake by control cells (a) and by cells treated with 25 (b), 50 (c), and 100 µg/ml (d) of ZnONPs, respectively, for 24 h. In (II), orange, red, and green colors represent 3, 6, 24 h, respectively; In (IIIA), pink, blue, and orange colors represent 3, 6, 24 h, respectively. NC denotes negative control. Magnification of the image in IIIB: 40×. In (II) and (IIIA): *, $p < 0.05$; **, $p < 0.01$.

aments. Actin filaments of the cells were stained red with the florescent dye rhodamine and counter stained with DAPI, thereby emitting blue fluorescence. When compared to control, significant rearrangement of cytoskeleton and rounding up of the cells were observed at 50 and 100 µg/ml of ZnONPs. In addition, actin filaments showed relatively more condensation at higher concentrations of ZnONPs than control cells (**Figure 2b**).

3.3. ROS Formation

The intensity of green fluorescence emitted by DCF associated with ROS generation after exposure of the cells to ZnONPs for 3, 6, and 24 h was analyzed. Compared to control, the ROS levels in cells treated with ZnONPs increased in a concentration- and time-dependent manner (**Figure 3a**). **Figure 3b** shows representative microphotographs of DCFH-DA-stained cells after exposure to ZnONPs at 0, 5, 15, 25, 50, and 100 µg/ml, respectively, for 24 h.

3.4. Lysosomal Integrity

The effect of ZnONPs on lysosomal membrane integrity of CHO cells was analyzed by staining with acridine orange. Acridine orange emits red fluorescence under acidic conditions when the lysosomes are intact. This can be visualized in control cells and at low concentrations of ZnONPs. However, the loss of lysosomal membrane integrity shifts the intensity of red lysosomal acridine orange to green. It was clearly visible at higher concentrations (50 and 100 µg/ml) of ZnONPs. **Figure 4a** shows the microphotographs of the cells stained with acridine orange. There was only a minor increase in loss of lysosomal membrane integrity by ZnONPs at 3 and 6 h, which was statistically insignificant. After 24 h exposure,

©2019 AIMSCI Inc. All Rights Reserved.

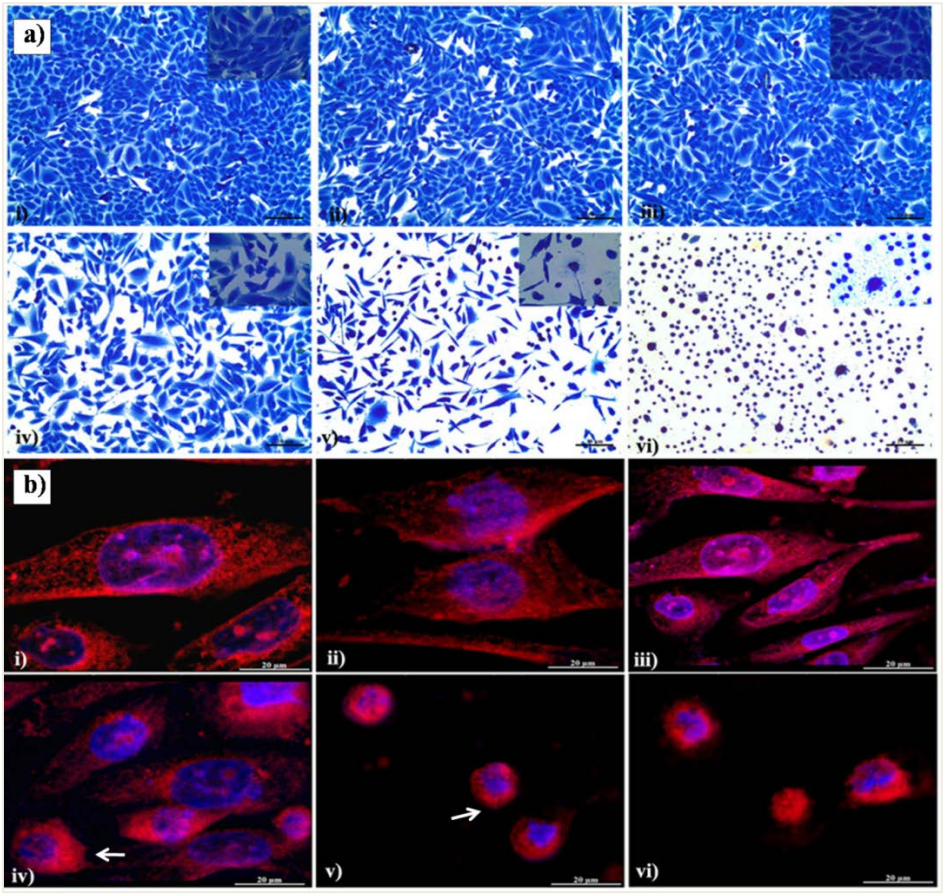

FIGURE 2. Effects of ZnONPs on CHO cell morphology. a: Representative microphotographs of Coomassie Brilliant blue staining of CHO cells after treatment with ZnONPs at 0 (i), 5 (ii), 15 (iii), 25 (iv), 50 (v), and 100 µg/ml (vi) for 24 h (scale bar, 100 µm; magnification, 20×). For inserted images: scale bar, 50 µm; magnification, 40×. b: Actin staining of CHO cells after treatment with ZnONPs at 0 (i), 5 (ii), 15 (iii), 25 (iv), 50 (v), and 100 µg/ml (vi) for 24 h (scale bar, 20 µm; magnification, 100×).

significant rise in green florescence was observed. Quantitative assessment of acridine orange staining was determined using the U.S. NIH ImageJ software (Bethesda, MD, USA) and is presented in **Figure 4c**.

3.5. Mitochondrial Membrane Potential

JC1 staining was adopted for examining the mitochondrial membrane potential (MMP) inside the cells before and after treatment with ZnONPs. A decrease in MMP was observed in ZnONPs-treated cells. As shown in **Figure 4b**, both control and cells treated with lower concentrations of ZnONPs emit red fluorescence. At higher concentrations, the cells lost its MMP and were observed to emit green fluorescence. **Figure 4d** shows the quantitative determination of fluorescence intensity in JC1 staining using the U.S. NIH ImageJ software.

3.6. Nuclear Condensation

Possible anomalies induced by ZnONPs in nuclear premises was evaluated using DAPI staining and cells were counter stained with acridine orange for convenience in visibility. There was no marked change in the nuclear morphology at 5 and 15 µg/ml

©2019 AIMSCI Inc. All Rights Reserved.

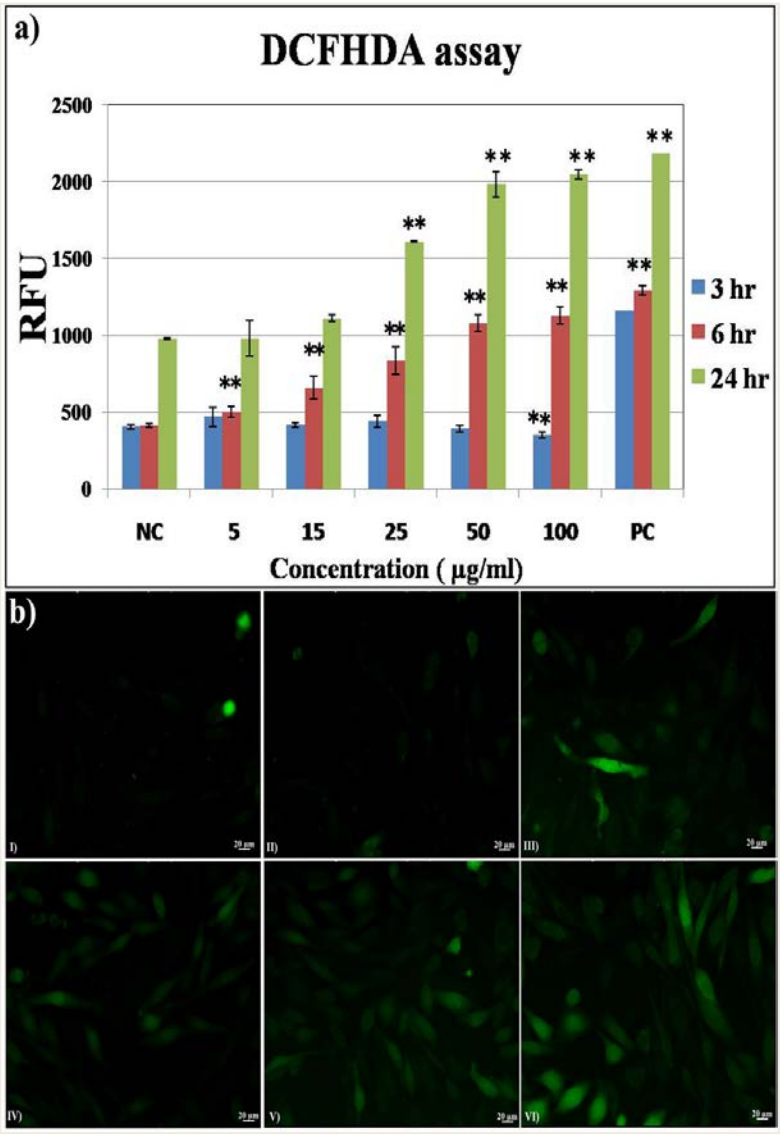

FIGURE 3. ROS generation in CHO cells after treatment with ZnONPs. a: Quantitative analysis of DCF fluorescence intensity. Values are expressed in relative fluorescent units (RFU). *, $p < 0.05$; **, $p < 0.01$. b: Representative microphotographs of DCF fluorescence in cells after treatment with ZnONPs at 0 (i), 5 (ii), 15 (iii), 25 (iv), 50 (v), and 100 µg/ml (vi) for 24 h (scale bar, 20 µm; magnification, 20×).

of ZnONPs with respect to control. Nuclear condensation was found to occur at 25 and 50 µg/ml and cell nucleus showed shrinkage and condensed chromatin at 100 µg/ml of ZnONPs (**Figure 5a**). Fluorescence intensity of DAPI staining was assessed using the U.S. NIH ImageJ software and is shown in **Figure 5c**.

3.7. Necrosis and Apoptosis

AO/EtBr dual staining was used to analyze the intensity of necrosis associated with ZnONPs treatment for 24 h. Acridine orange stains both live and dead cells whereas EtBr stains those cells undergoing necrosis. Viable control cells were discernibly visible

©2019 AIMSCI Inc. All Rights Reserved.

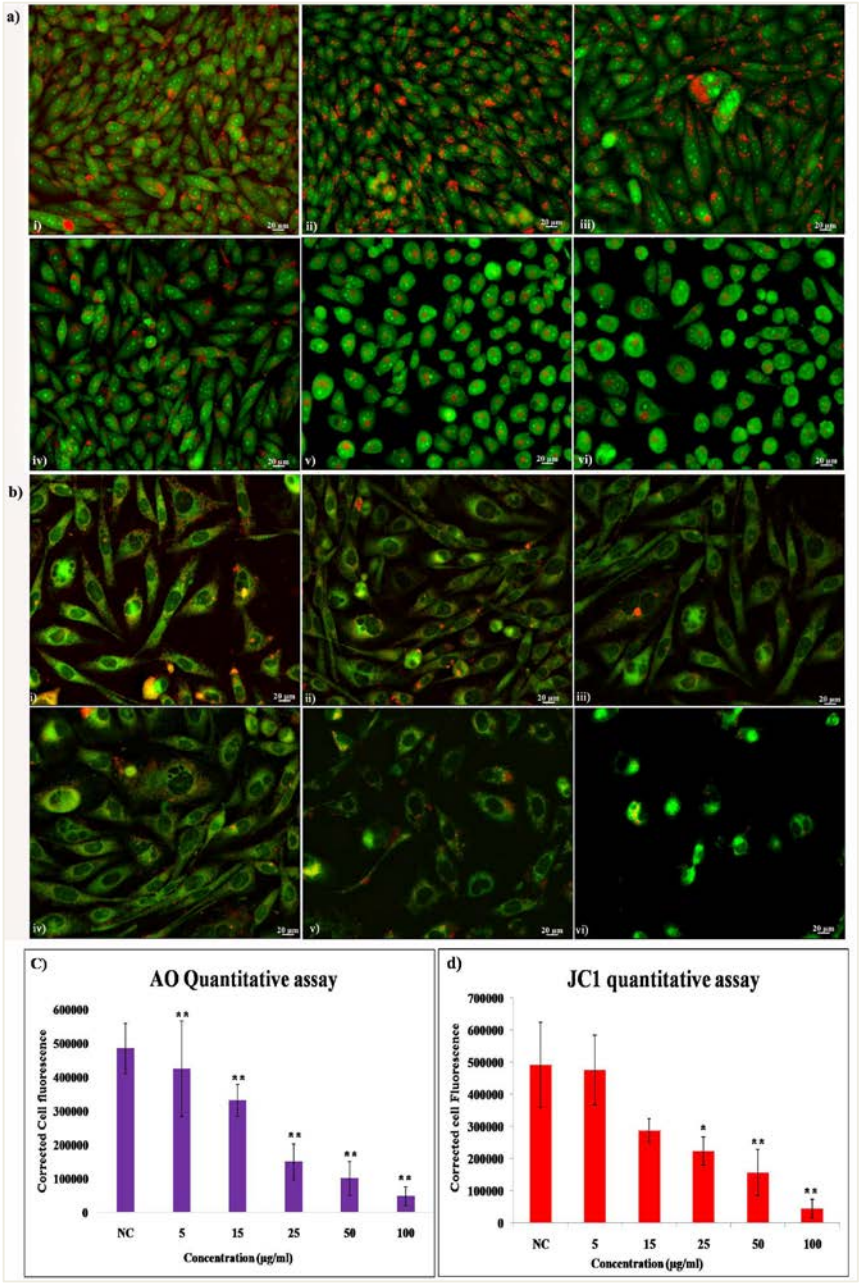

FIGURE 4. Effects of ZnONPs on lysosomal membrane integrity and MMP in CHO cells. a: Lysosomal membrane integrity of CHO cells after 24 h exposure to ZnONPs at 0 (i), 5 (ii), 15 (iii), 25 (iv), 50 (v), and 100 µg/ml (vi), as assessed by acridine orange staining (scale bar, 20 µm; magnification, 20×). In acid vesicles like lysosomes, acridine orange emits orange to red fluorescence against the green cytoplasm. In cells having destabilized lysosomes, the red fluorescence shifts to green. b: MMP assessed by using JC1 dye in CHO cells after 24 h exposure to ZnONPs at 0 (i), 5 (ii), 15 (iii), 25 (iv), 50 (v), and 100 µg/ml (vi) (scale bar, 20 µm; magnification, 20×). JC1 emits green fluorescence in depolarized mitochondria, whereas in active mitochondria, JC1 aggregates emit orange to red fluorescence. c: Quantitative assessment of acridine orange staining. d: Quantitative assessment of JC1 staining. In b and c: *, $p < 0.05$; **, $p < 0.01$.

©2019 AIMSCI Inc. All Rights Reserved.

with intense green fluorescence provided by acridine orange. Similar trend was observed for cells exposed to 5 and 15 μg/ml ZnONPs. Relative to control, a concentration-dependent increase in EtBr-positive cells was observed from 25 μg/ml onwards. At 50 μg/ml of ZnONPs, the cells displayed an intense shift from green to orange color and morphological features which are characteristics of apoptosis including blebbing and cell shrinkage. At 100 μg/ml, the cells underwent necrotic death and exhibited red fluorescence (**Figure 5b**). Quantitative fluorescence measurement of AO/EtBr staining from the U.S. NIH ImageJ software is shown in **Figure 5d**.

With live/dead assay of the cells, it was observed that low (5 μg/ml) and medium (25 μg/ml) concentrations of ZnONPs treatment for 24 h had no significant induction of apoptotic/necrotic cell death compared to control. However, a drastic increase in apoptotic and necrotic cell death was observed at 100 μg/ml: 30% and 50% of cells underwent apoptotic and necrotic cell death, respectively (**Figure 6**).

4. DISCUSSION

Material science engineering at the nanometer level led to the nourishment of scientific research in different biomedical, electronic, and industrial scenarios. Unique photochemical properties of ZnONPs turned it to be the most promising nanomaterial in the production of cosmetic, electronic, and biomedical products worldwide. Despite the widespread use, the safety of these NPs in human body has not yet fully established. Recently, reports highlighted that the extreme solubility and dissolution property of ZnONPs elicit developmental toxicity in aquatic animals by altering expression of genes necessary for their development and immune signaling [23]. The present study focused on the bio-nano interaction of ZnONPs with the CHO cell line.

It is difficult to assess the toxicity of NPs in biological system via a single assay. Therefore, combination of assays analyzing changes in morphology, organelle functions, and nuclear condensation were carried out. Kang et al. in 2013 performed the MTT assay to assess the viability of Caco-2 cells after ZnONPs exposure. After an ideal time of exposure, it was observed that maximum toxicity was produced by smaller sized particles in a time- and concentration-dependent manner [24]. Comparable to that observation, the present study also showed concentration- and time-dependent cytotoxicity of ZnONPs in CHO cells. Both MTT and neutral red uptake assays showed similar trend, with adverse effect of ZnONPs on viability of cells, which was initiated after 6 h of exposure. Almost 80% of cells lost its viability at 100 μg/ml after 24 h exposure. However, a contradictory observation was obtained for the MTT assay wherein 5 and 15 μg/ml ZnONPs exposure for 6 h caused slight increase in cell viability. Similar result has previously been reported by Ong et al. [25]. There exists a prospect for such an observation due to nanoparticle interference with assay reagents. Likewise, the neutral red uptake assay also exhibited the same inclination except the fact that it occurred only for 15 μg/ml during 6 h exposure.

Cellular uptake and intracellular fate of NPs depends on their size, charge, and shape, as well as the type of cells with which they interact. Interaction of NPs with cellular membrane proteins may result in loss of functionality or membrane integrity [26]. Regarding morphological evaluation of ZnONPs-exposed cells in the present study, untreated cells in the control group were normally spindle or polygonal in morphology. However, at higher concentrations of ZnONPs treatment, the cells lost their adhering capacity and changed the characteristic polygonal shape into completely round as also reported by Wang et al. with LTEP-a-2 cells [27]. Paszek et al. demonstrated that ZnONPs exhibited time- and dose-dependent disruption of human umbilical vein endothelial cell (HUVEC) membrane associated with F actin re-localization and destabilization of intercellular contact [28]. The size, density, and surface homogeneity of HUVEC cells were significantly affected by ZnONPs treatment for longer duration. In the same way, the present study showed significant loss of cytoskeletal integrity of CHO cells with disorganization of actin filaments in a time- and concentration-dependent manner.

The partial dissolution in aqueous environment and metal ion releasing nature of ZnONPs made them more cytotoxic to bacterial as well as mammalian cells. The mechanism of cell membrane interaction, internalization, ROS generation, and lysosomal and mitochondrial damage marks the harmful effect of these NPs in living cells [29]. Here also a concentration- and time-dependent increase in ROS levels was observed during cellular exposure to ZnONPs for 6 and 24 h. Despite this fact, an ambiguous result

©2019 AIMSCI Inc. All Rights Reserved.

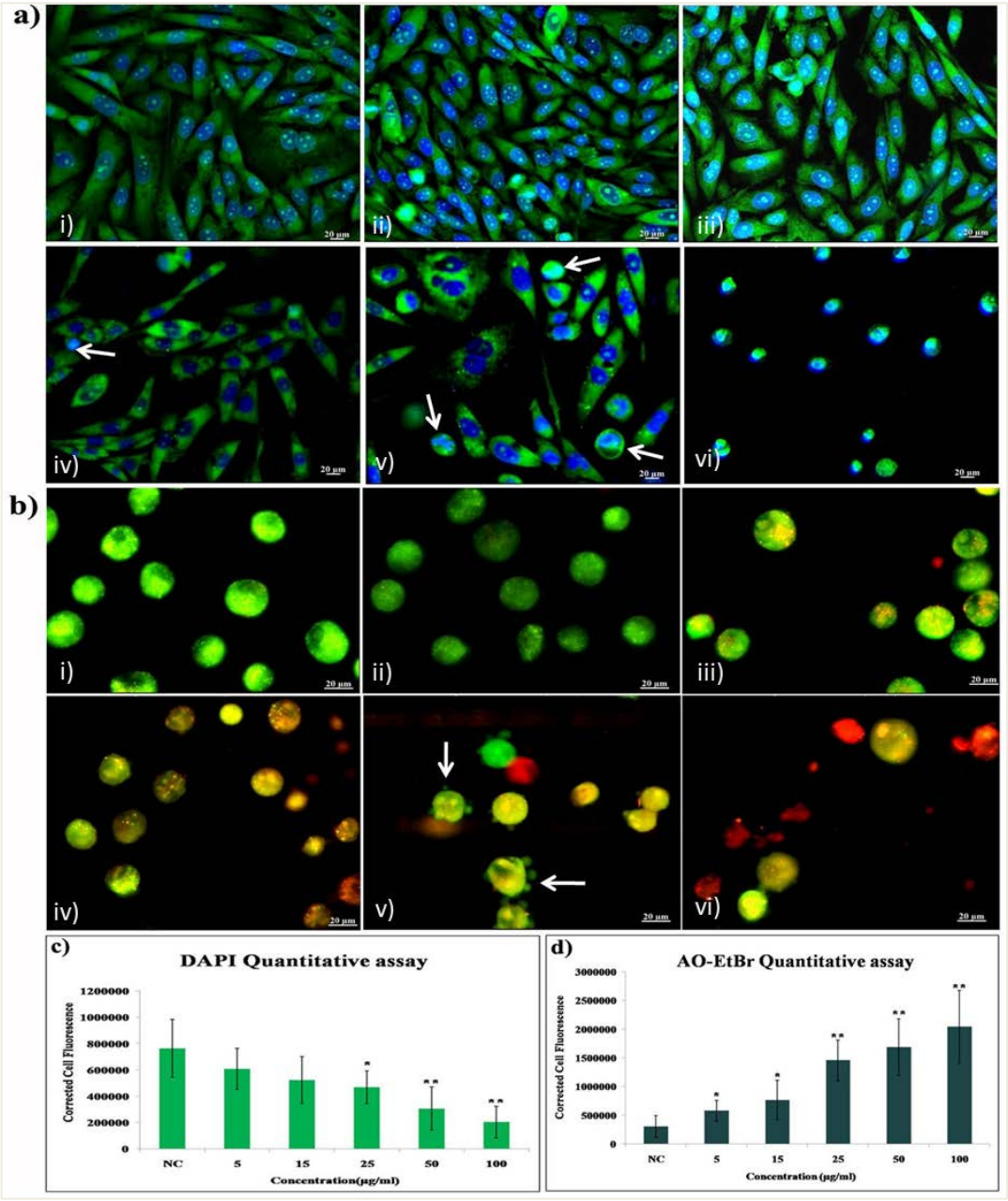

FIGURE 5. Nuclear condensation and necrosis in ZnONPs-treated CHO cells. a: Analysis of nuclear condensation in CHO cells after 24 h exposure with ZnONPs at 0 (i), 5 (ii), 15 (iii), 25 (iv), 50 (v), and 100 µg/ml (vi). The nucleus was stained with blue fluorescent stain DAPI and the cytoplasm was counter stained using acridine orange. Arrow indicates condensed nucleus (scale bar, 20 µm; magnification, 20×). b: AO-EtBr dual staining for necrosis analysis in CHO Cells after 24 h treatment with ZnONPs at 0 (i), 5 (ii), 15 (iii), 25 (iv), 50 (v), and 100 µg/ml (vi). Healthy cells stained with acridine orange emitted green fluorescence. Necrotic cells took up ethidium bromide and emitted red fluorescence. Arrow indicates characteristic blebbing of apoptotic cells (scale bar, 20 µm; magnification, 20×). c: Quantitative assessment of DAPI staining. d: Quantitative assessment of AO-EtBr staining. In b and c: *, $p < 0.05$; **, $p < 0.01$.

©2019 AIMSCI Inc. All Rights Reserved.

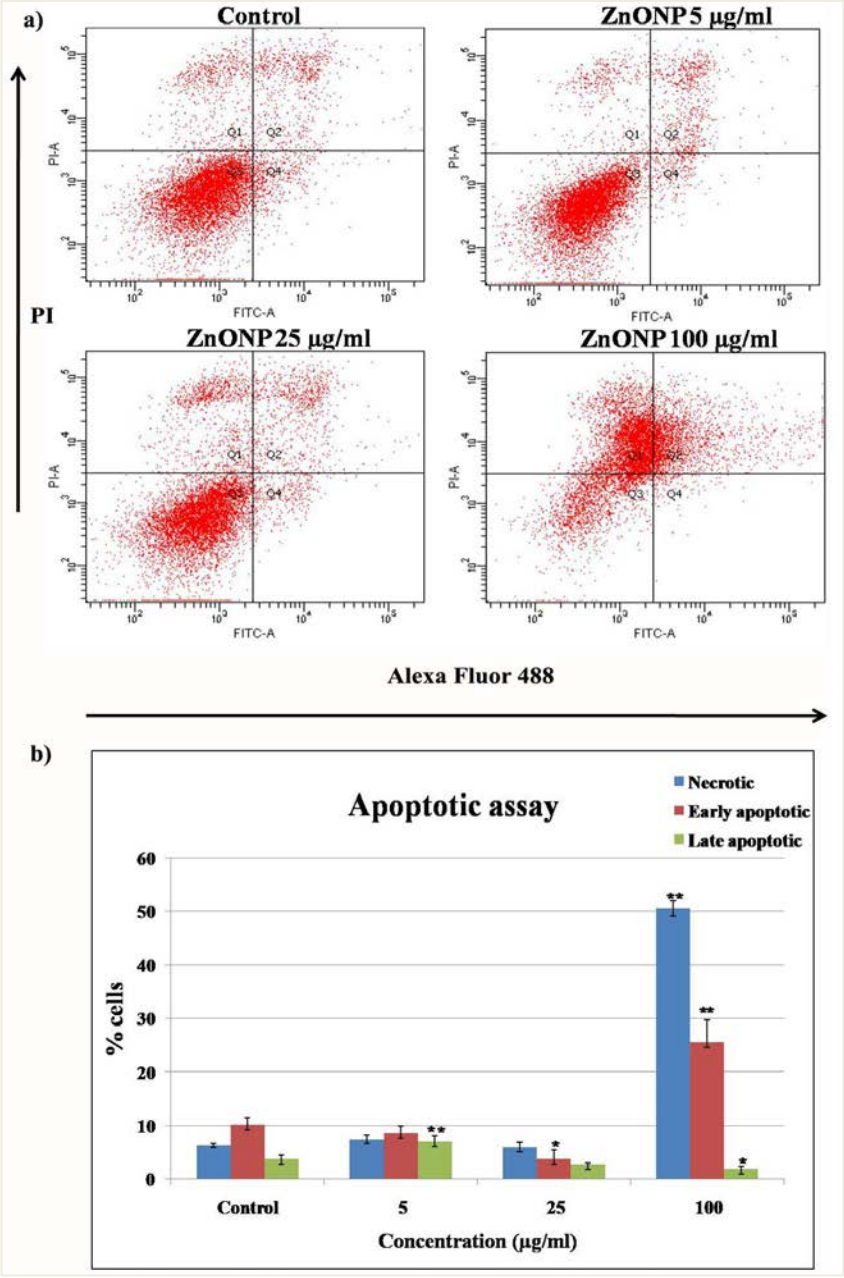

FIGURE 6. Flow cytometry of CHO cells treated with the indicated concentrations of ZnONPs for 24 h. a: Flow cytograms showing apoptosis/necrosis. Q1, necrotic cells; Q2, late apoptotic cells; Q3, live cells; and Q4, early apoptotic cells. b: Graphical representation of percentage of cells undergoing necrosis, early apoptosis, and late apoptosis. *, $p < 0.05$; **, $p < 0.01$.

showing decline in ROS levels during 3 h exposure could be attributed to free radical scavenging property of ZnONPs as reported earlier by Siregar et al. [30]. On the other hand, prolonged cellular exposure

©2019 AIMSCI Inc. All Rights Reserved.

outweighed this scavenging property as evident from rise in ROS levels.

Here also the result obtained from DCFH-DA assay indicated that ROS generation has significant role in toxicity of ZnONPs in a concentration-dependent manner. Initially, cells showed an immediate antioxidant response after particle exposure for 3 h. Prolonged incubation with ZnONPs attenuated the antioxidant defense mechanism of the cells. Recent reports suggest that ZnONPs induced generation of ROS and the formed ROS are the major reason behind impairment of oxidative stress management machinery in cells. ROS can mediate multiple damages including rupturing of cell membrane, disturbed structural dynamics of cytoskeleton, mitochondrial dysfunctions, and global DNA demethylation [31].

Any compound that alters MMP may results in free radical generation and associated cell death. In 2012, Li et al. studied the toxic effect of ZnONPs on liver mitochondria isolated from Wistar rats by analyzing effects on MMP, membrane ultrastructure, permeabilization to H^+ and K^+ ions, mitochondrial respiration, and release of cytochrome c as a marker of apoptotic signaling [32]. It was reported that Zn^{2+} ions released from ZnONPs critically affected the functioning of mitochondrial respiratory chain and membrane permeability, and ultimately resulted in ROS generation and associated cell death. In the present study, the JC1 fluorescent probe was used as a marker of MMP analysis. The present study confirmed the decrease in MMP after exposure to ZnONPs in a time- and concentration-dependent manner.

Acridine orange and neutral red uptake assays are suitable to analyze the functional activity of lysosomes. It was reported that lysosomal dysfunction with loss of membrane integrity was one of the important causes of cell death in HepG2 cells after ZnONPs treatment for 3 to 24 h [33]. Lysosomes within a healthy cell have an acidic pH wherein acridine orange emits red fluorescence. However, the loss of membrane integrity results in translocation of lysosomal contents into the cytosol. Disintegrated lysosomes in the cytoplam experience shift of acidic pH to alkaline range. Acridine orange emits green fluorescence at alkaline condition. Lysosomal destabilization and release of proteolytic enzymes by metal oxide NPs have already been reported by several studies in fibroblast, macrophages, and bronchial epithelial cells [34, 35]. Similarly, for the present study, both qualitative and quantitative analysis using acridine orange staining indicated that ZnONPs could induce lysosomal dysfunction in a time- and concentration-dependent way. The dissolution of ZnONPs in the acidic compartment enhances the release of Zn^{2+} ions into the cell cytoplasm, which may be responsible for the production of ROS. Impaired autophagic flux and autophagosome formation may thus lead to non-apoptotic cell death.

Han et al. showed the DNA breakage in mouse testicular cells treated with rod shaped ZnONPs of approximately 70 nm size using DAPI and γ-H2AX, a marker of DNA double-strand breaks [36]. Despite of chromatin condensation, the present study did not show any DNA double-strand breaks. Blockage of both γ-H2AX and NF-κB by ZnONPs within CHO-K1 cells and chicken embryo was reported by Liu et al. proposing the potential anti-proliferative and apoptotic role of ZnONPs at embryonic developmental stage [37]. Dual AO-EtBr florescent probes are suitable for distinguishing live and apoptotic cells. Acridine orange is a vital stain that stains both live and dead cells whereas EtBr is a DNA intercalating agent that stains only those cells undergoing necrosis [38]. Here the EtBr was capable of entering the cells indicating initial stage of apoptosis in response to ZnONPs of 25 μg/ml onwards. This proved the loss of membrane integrity due to cellular stress. Intense red fluorescence obtained at 50 μg/ml ZnONPs indicated necrotic cell death.

Apoptosis is a normal homeostatic mechanism during development and aging processes. The fate of a cell to undergo apoptotic or necrotic death depends on the nature of the death signal, the tissue type, the developmental stage of the tissue, and the physiological milieu. Here, from the annexin V/PI flow cytometry analysis, it was observed that low and medium concentrations of ZnONPs treatment induced mild apoptotic signaling where at high concentrations, cells underwent apoptotic as well as necrotic death. More than 50% of cells were subjected to necrotic disintegration and 35% were in early apoptotic stage, implicating the potential toxicity of ZnONPs. These results are in harmony with the findings of Boroumand et al. that ZnONPs induced apoptosis in MCF-7 cells with significant upregulation of pro-apoptotic factors (p53, p21, Bax, and JNK) and downregulation of anti-apoptotic factors (Bcl-2, AKT1, and ERK1/2) in a concentration-dependent manner [39]. Oxidative stress may play a crucial role

©2019 AIMSCI Inc. All Rights Reserved.

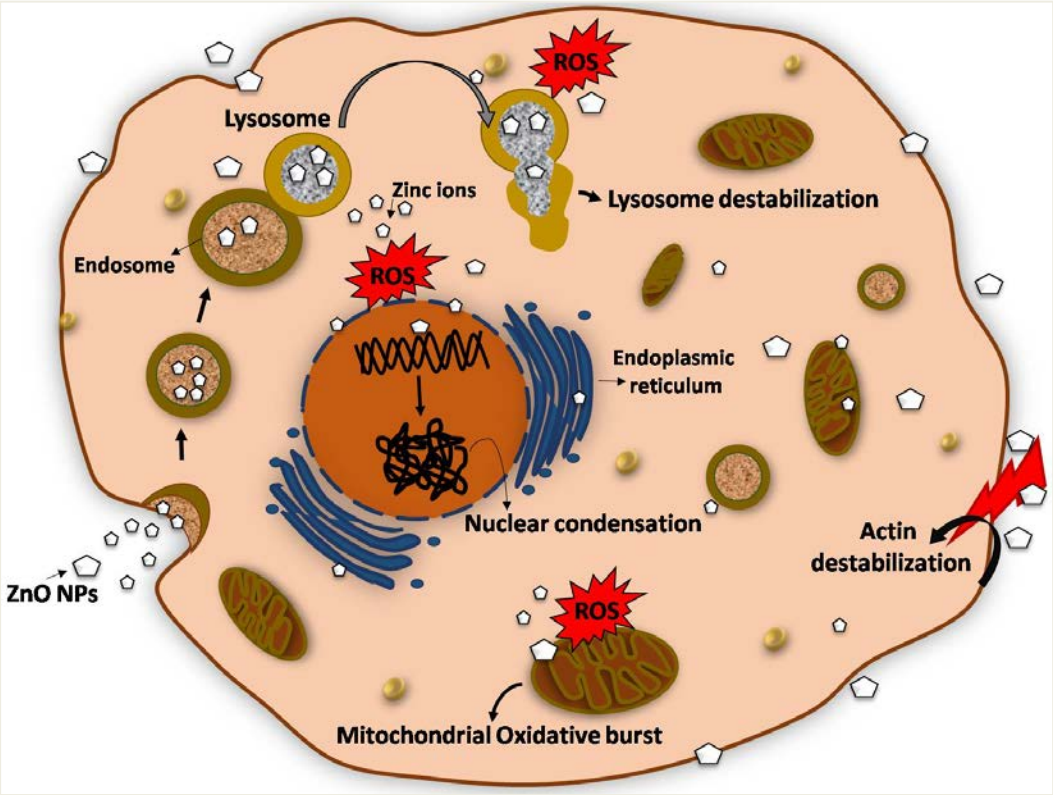

FIGURE 7. Diagrammatic illustration of ZnONPs-induced cytotoxicity in CHO cells. As illustrated, ZnONPs target diverse intracellular structural components and oxidative stress may be a critical mechanism leading to the eventual death of the cells.

in ZnONPs-mediated apoptosis in which concentration-dependent generation of ROS affects MMP and initiates mitochondria mediated apoptosis. According to Wang et al. a concentration-dependent increase in the phosphorylation of JNK, ERK, and p38 MAPK indicated a role of ZnONPs in inducing enhancement of stress-activated protein kinases in primary astrocytes. The nuclear condensation, poly(ADP-ribose)polymerase-1 (PARP) cleavage, and cleaved caspase-3 expression, as well as the concomitant increase in the expression of Bax/Bcl-2 ratio in astrocytes also suggest the JNK-mediated apoptotic signaling following exposure to ZnONPs [40]. Apart from available study reports regarding the developmental and reproductive toxicity of ZnONPs in marine ecosystem, the present study provided molecular insights into ZnONPs-induced subcellular structural damage in a mammalian ovarian cell line.

5. CONCLUSION

In the present study, interaction of ZnONPs with an ovarian cell line was analyzed. ZnONPs attracted the field of nanotechnology with their unique physicochemical and dissolution properties. They were credited in the areas including rubber industry, cosmetics, electronics, and biomedical technology. The present study showed that ZnONPs affected the viability and morphology of CHO cells in a concentration- and time-dependent manner. Interaction of ZnONPs with cell membrane resulted in destabilization of structural filaments. Internalized ZnONPs induced oxidative stress and associated damage to cell organelles like mitochondria and lysosomes. ROS generation might lead to loss of MMP and subsequently trigger apoptotic signaling in CHO cells. At very high concentrations (e.g., 100 µg/ml) of ZnONPs, cells underwent

©2019 AIMSCI Inc. All Rights Reserved.

energy independent necrotic death with bursting of cells via membrane destruction. ZnONPs caused condensation of chromosomes at higher concentrations. Hence, as depicted in **Figure 7**, the present study demonstrated detailed cytotoxic effects of ZnONPs in an ovarian cell line, likely via an oxidative stress mechanism.

ACKNOWLEDGMENTS

The authors are thankful to the Director and Head of Biomedical Technology Wing, Sree Chitra Tirunal Institute for Medical Sciences and Technology for providing the facilities to carry out the work. N.P. and S.S.A. thank the CSIR (New Delhi, India) for the Junior Research Fellowship. The authors declare no conflicts of interest.

REFERENCES

1. Sharma D, Kanchi S, Bisetty K. Biogenic synthesis of nanoparticles: a review. *Arab J Chem* 2015. doi: 10.1016/j.arabjc.2015.11.002.
2. Armstead AL, Li B. Nanotoxicity: emerging concerns regarding nanomaterial safety and occupational hard metal (WC-Co) nanoparticle exposure. *Int J Nanomedicine* 2016; 11:6421–33. doi: 10.2147/IJN.S121238.
3. Zhang Y, Nayak TR, Hong H, Cai W. Biomedical applications of zinc oxide nanomaterials. *Curr Mol Med* 2013; 13(10):1633–45.
4. Kolodziejczak-Radzimska A, Jesionowski T. Zinc oxide-from synthesis to application: a review. *Materials (Basel)* 2014; 7(4):2833–81. doi: 10.3390/ma7042833.
5. Rajput VD, Minkina TM, Behal A, Sushkova SN, Mandzhieva S, Singh R, et al. Effects of zinc-oxide nanoparticles on soil, plants, animals and soil organisms: a review. *Environ Nanotechnol Monit Manage* 2018; 9:76–84.
6. Renzi M, Guerranti C. Ecotoxicity of nanoparticles in aquatic environments: a review based on multivariate statistics of meta-data. *J Environ Anal Chem* 2015; 2(4):149. doi: 10.4172/2380-2391.1000149.
7. Wang CC, Wang S, Xia Q, He W, Yin JJ, Fu PP, et al. Phototoxicity of zinc oxide nanoparticles in HaCaT keratinocytes-generation of oxidative DNA damage during UVA and visible light irradiation. *J Nanosci Nanotechnol* 2013; 13(6):3880–8. doi: 10.1166/jnn.2013.7177.
8. Yan G, Huang Y, Bu Q, Lv L, Deng P, Zhou J, et al. Zinc oxide nanoparticles cause nephrotoxicity and kidney metabolism alterations in rats. *J Environ Sci Health A Tox Hazard Subst Environ Eng* 2012; 47(4):577–88. doi: 10.1080/10934529.2012.650576.
9. Mansouri E, Khorsandi L, Orazizadeh M, Jozi Z. Dose-dependent hepatotoxicity effects of zinc oxide nanoparticles. *Nanomedicine J* 2015; 2(4):273–82.
10. Sruthi S, Mohanan PV. Investigation on cellular interactions of astrocytes with zinc oxide nanoparticles using rat C6 cell lines. *Colloids Surf B Biointerfaces* 2015; 133:1–11. doi: 10.1016/j.colsurfb.2015.05.041.
11. Heng BC, Zhao X, Xiong S, Ng KW, Boey FY, Loo JS. Toxicity of zinc oxide (ZnO) nanoparticles on human bronchial epithelial cells (BEAS-2B) is accentuated by oxidative stress. *Food Chem Toxicol* 2010; 48(6):1762–6. doi: 10.1016/j.fct.2010.04.023.
12. Pati R, Das I, Mehta RK, Sahu R, Sonawane A. Zinc-Oxide nanoparticles exhibit genotoxic, clastogenic, cytotoxic and actin depolymerization effects by inducing oxidative stress responses in macrophages and adult mice. *Toxicol Sci* 2016; 150(2):454–72. doi: 10.1093/toxsci/kfw010.
13. Zhang W, Bao S, Fang T. The neglected nano-specific toxicity of ZnO nanoparticles in the yeast *Saccharomyces cerevisiae*. *Sci Rep* 2016; 6:24839. doi: 10.1038/srep24839.
14. Syama S, Sreekanth PJ, Varma HK, Mohanan PV. Zinc oxide nanoparticles induced oxidative stress in mouse bone marrow mesenchymal stem cells. *Toxicol Mech Methods* 2014; 24(9):644–53. doi: 10.3109/15376516.2014.956914.
15. Bahuguna A, Khan I, Bajpai VK, Kang SC. MTT assay to evaluate the cytotoxic potential of a drug. *Bangladesh J Pharmacol* 2017; 12(2):115–8.
16. Repetto G, del Peso A, Zurita JL. Neutral red uptake assay for the estimation of cell viability/cytotoxicity. *Nat Protoc* 2008; 3(7):1125–31. doi: 10.1038/nprot.2008.75.
17. Reshma SC, Syama S, Mohanan PV. Nano-

©2019 AIMSCI Inc. All Rights Reserved.

biointeractions of PEGylated and bare reduced graphene oxide on lung alveolar epithelial cells: A comparative in vitro study. *Colloids Surf B Biointerfaces* 2016; 140:104–16. doi: 10.1016/j.colsurfb.2015.12.030.
18. Latvala S, Hedberg J, Di Bucchianico S, Moller L, Odnevall Wallinder I, Elihn K, et al. Nickel release, ros generation and toxicity of Ni and NiO micro- and nanoparticles. *PLoS One* 2016; 11(7):e0159684. doi: 10.1371/journal.pone.0159684.
19. Perelman A, Wachtel C, Cohen M, Haupt S, Shapiro H, Tzur A. JC-1: alternative excitation wavelengths facilitate mitochondrial membrane potential cytometry. *Cell Death Dis* 2012; 3:e430. doi: 10.1038/cddis.2012.171.
20. Sohaebuddin SK, Tang L. A simple method to visualize and assess the integrity of lysosomal membrane in mammalian cells using a fluorescent dye. In: *Cellular and Subcellular Nanotechnology* (V Weissig, T Elbaypumi, M Olsen). Humana Press, Totowa, NJ, 2013, pp. 25–31.
21. Tone S, Sugimoto K, Tanda K, Suda T, Uehira K, Kanouchi H, et al. Three distinct stages of apoptotic nuclear condensation revealed by time-lapse imaging, biochemical and electron microscopy analysis of cell-free apoptosis. *Exp Cell Res* 2007; 313(16):3635–44. doi: 10.1016/j.yexcr.2007.06.018.
22. Liu K, Liu PC, Liu R, Wu X. Dual AO/EB staining to detect apoptosis in osteosarcoma cells compared with flow cytometry. *Med Sci Monit Basic Res* 2015; 21:15–20. doi: 10.12659/MSMBR.893327.
23. Choi JS, Kim RO, Yoon S, Kim WK. Developmental toxicity of zinc oxide nanoparticles to zebrafish (*Danio rerio*): a transcriptomic analysis. *PLoS One* 2016; 11(8):e0160763. doi: 10.1371/journal.pone.0160763.
24. Kang T, Guan R, Chen X, Song Y, Jiang H, Zhao J. In vitro toxicity of different-sized ZnO nanoparticles in Caco-2 cells. *Nanoscale Res Lett* 2013; 8(1):496. doi: 10.1186/1556-276X-8-496.
25. Ong KJ, MacCormack TJ, Clark RJ, Ede JD, Ortega VA, Felix LC, et al. Widespread nanoparticle-assay interference: implications for nanotoxicity testing. *PLoS One* 2014; 9(3):e90650. doi: 10.1371/journal.pone.0090650.
26. Behzadi S, Serpooshan V, Tao W, Hamaly MA, Alkawareek MY, Dreaden EC, et al. Cellular uptake of nanoparticles: journey inside the cell. *Chem Soc Rev* 2017; 46(14):4218–44. doi: 10.1039/c6cs00636a.
27. Wang C, Hu X, Gao Y, Ji Y. ZnO nanoparticles treatment induces apoptosis by increasing intracellular ROS levels in LTEP-a-2 cells. *Biomed Res Int* 2015; 2015:423287. doi: 10.1155/2015/423287.
28. Paszek E, Czyz J, Woznicka O, Jakubiak D, Wojnarowicz J, Lojkowski W, et al. Zinc oxide nanoparticles impair the integrity of human umbilical vein endothelial cell monolayer in vitro. *J Biomed Nanotechnol* 2012; 8(6):957–67.
29. Stankic S, Suman S, Haque F, Vidic J. Pure and multi-metal oxide nanoparticles: synthesis, antibacterial and cytotoxic properties. *J Nanobiotechnology* 2016; 14(1):73. doi: 10.1186/s12951-016-0225-6.
30. Siregar TM, Cahyana AH, Gunawan RJ. Characteristics and free radical scavenging activity of zinc oxide (ZnO) nanoparticles derived from extract of coriander (*Coriandrum sativum* L.). *Reaktor* 2017; 17(3):145–50.
31. Choudhury SR, Ordaz J, Lo CL, Damayanti NP, Zhou F, Irudayaraj J. From the Cover: Zinc oxide nanoparticles-induced reactive oxygen species promotes multimodal cyto- and epigenetic toxicity. *Toxicol Sci* 2017; 156(1):261–74. doi: 10.1093/toxsci/kfw252.
32. Li JH, Liu XR, Zhang Y, Tian FF, Zhao GY, Jiang FL, et al. Toxicity of nano zinc oxide to mitochondria. *Toxicol Res* 2012; 1(2):137–44.
33. Zhou Y, Fang X, Gong Y, Xiao A, Xie Y, Liu L, et al. The Interactions between ZnO nanoparticles (NPs) and alpha-linolenic acid (LNA) complexed to BSA did not influence the toxicity of ZnO NPs on HepG2 cells. *Nanomaterials (Basel)* 2017; 7(4). doi: 10.3390/nano7040091.
34. Sohaebuddin SK, Thevenot PT, Baker D, Eaton JW, Tang L. Nanomaterial cytotoxicity is composition, size, and cell type dependent. *Part Fibre Toxicol* 2010; 7:22. doi: 10.1186/1743-8977-7-22.
35. Hussain S, Thomassen LC, Ferecatu I, Borot MC, Andreau K, Martens JA, et al. Carbon black and titanium dioxide nanoparticles elicit distinct

©2019 AIMSCI Inc. All Rights Reserved.

apoptotic pathways in bronchial epithelial cells. *Part Fibre Toxicol* 2010; 7:10. doi: 10.1186/1743-8977-7-10.

36. Han Z, Yan Q, Ge W, Liu ZG, Gurunathan S, De Felici M, et al. Cytotoxic effects of ZnO nanoparticles on mouse testicular cells. *Int J Nanomedicine* 2016; 11:5187–203. doi: 10.2147/IJN.S111447.
37. Liu J, Zhao Y, Ge W, Zhang P, Liu X, Zhang W, et al. Oocyte exposure to ZnO nanoparticles inhibits early embryonic development through the gamma-H2AX and NF-kappaB signaling pathways. *Oncotarget* 2017; 8(26):42673–92. doi: 10.18632/oncotarget.17349.
38. Kavithaa K, Paulpandi M, Ponraj T, Murugan K, Sumathi S. Induction of intrinsic apoptotic pathway in human breast cancer (MCF-7) cells through facile biosynthesized zinc oxide nanorods. *Karbala Int J Modern Sci* 2016; 2(1):46–55.
39. Boroumand Moghaddam A, Moniri M, Azizi S, Abdul Rahim R, Bin Ariff A, Navaderi M, et al. Eco-friendly formulated zinc oxide nanoparticles: induction of cell cycle arrest and apoptosis in the MCF-7 cancer cell line. *Genes (Basel)* 2017; 8(10). doi: 10.3390/genes8100281.
40. Wang J, Deng X, Zhang F, Chen D, Ding W. ZnO nanoparticle-induced oxidative stress triggers apoptosis by activating JNK signaling pathway in cultured primary astrocytes. *Nanoscale Res Lett* 2014; 9(1):117. doi: 10.1186/1556-276X-9-117.

©2019 AIMSCI Inc. All Rights Reserved.